

Development of Small-Scale Arc-jet Facility OPG1

Tobias A. Hermann*, Eric Won Keun Chang†, Joelle Schäfer‡ and Chinmay Joglekar§
Oxford Thermofluids Institute, University of Oxford, Southwell Building, Osney Mead, OX2 0ES Oxford, United Kingdom.

Hannah Böhrk¶
Baden-Württemberg Cooperative State University Stuttgart, Rotebühlstraße 133, 70197 Stuttgart, Germany

A small-scale thermal arc-jet facility based on a 21.5 kW tungsten inert gas welding power supply has been developed. The design and simulations are presented here. The plasma generator is situated inside a vacuum vessel forming an Argon plasma with a mass flow rate of approximately 0.2 g/s. The vessel is evacuated by a series of pumps providing sufficient suction to keep the vessel below 125 Pa during continuous operation. The system is designed with regards to heat transfer and vacuum performance with the goal of keeping component temperatures pressures below critical values to prevent material failure and enable adequate vacuum. The thermal design of the plasma generator includes a water cooling circuit which keeps the copper anode below melting temperatures. A viscous reacting 2D axisymmetric simulation is carried out using Eilmer4 simulating the nozzle flow including the stagnation chamber and the free jet impinging onto a 40 mm diameter sphere-cone model. The simulations predict a maximum heat flux on the model surface of approximately 800 kW/m² when a plasma total temperature of 7400 K is assumed.

I. Nomenclature

A	=	Area
C	=	Vacuum conductance
d	=	Diameter
h	=	Heat transfer coefficient
k	=	Thermal conductivity
L	=	Length
l	=	Length
\dot{m}	=	Mass flow rate
Nu	=	Nusselt number
p	=	Pressure
Pr	=	Prandtl number
R	=	Electrical resistance
R	=	Specific gas constant
r	=	radius
Re	=	Reynolds number
T	=	Temperature
U	=	Thermal resistance
μ	=	Dynamic viscosity
ρ	=	Electrical resistivity

*Departmental Lecturer, University of Oxford, Oxford Thermofluids Institute, United Kingdom
†Postdoctoral research Assistant, University of Oxford, Oxford Thermofluids Institute, United Kingdom.
‡Masters Student, University of Stuttgart
§Masters Student, University of Oxford
¶Professor, Baden-Württemberg Cooperative State University Stuttgart, Stuttgart, Germany.

II. Introduction

Arc-jets are widely used in the experimental spacecraft entry community, mostly for the purpose of heat shield material validation and aerothermodynamic research [1–7]. Flows created by arc-jets simulate the high enthalpy flow found after the compression shock of a re-entry vehicle [8]. Large facilities allow for high heat flux conditions while providing high total pressure. These facilities require a large and varied support infrastructure such as a powerful multi-stage vacuum system, a power supply system capable of providing electric power in the megawatt order of magnitude, and a high-pressure water-cooling system to counteract the large heat loads on support structures such as mounting assemblies. They also require a high cost of operation and often have restricted availability for testing that isn't supported by a large research project, as pointed out in Ref [9]. Small-scale arc-jets allow for testing of new diagnostics or preliminary screening for material samples before their respective application in a large facility [10–12]. Small-scale facilities can achieve fast turn-around and relatively low cost operation and can be operated with fewer personnel.

The new plasma generator discussed in this paper adds an additional application of a small-scale arc-jet by using it as a pre-heating device, similar to the work presented in [13]. The envisioned methodology involves using a small arc-jet within the test section of an expansion tube facility to pre-heat a sub-scaled re-entry vehicle before it is exposed to the hypersonic flow. To the authors' knowledge, first mentioning of such a methodology was found in [14]. By manufacturing the capsule model from a heat shield material, ablation, blowing and plasma surface interaction can be simulated experimentally. The methodology is described in detail in an accompanying paper [15].

This work focusses on the development of the plasma generator as a stand-alone device to be used as a miniature plasma wind tunnel. This enables developing new plasma flow conditions required for the aforementioned pre-heating phase, characterisation of plasma flow parameters, diagnostic development, and small-scale material testing. The paper presents the experimental layout, the system design process, and CFD simulations of the generator nozzle.

III. Experimental setup

The facility is called Osney Plasma Generator 1 (OPG1) and is located in the Oxford Thermofluids Institute of the University of Oxford. It consists of a vacuum vessel in which the plasma generator is housed, a high throughput vacuum system, an electrical power supply, a water cooling system, a model mounting system, and a data acquisition system. The system is purposefully designed such that fast turn-around times between tests are possible. This includes a designed ease of access to models, the plasma generator, and the vacuum system. The powerful vacuum system and the small test section allows very fast evacuation of the vessel between tests. Additionally, the small-scale of the plasma generator allows a decoupling of the plasma torch from the vacuum vessel which is intended to decrease the likelihood of leaks from atmospheric air into the plasma source. This not only increases the purity of the plasma gas, but also protects the hot cathode from oxidation due to air ingress. In the following, an overview of the setup, the vacuum system, instrumentation layout, and plasma generator are given.

A. Overall layout

An overview of the core system is shown in Figs. 1, 2 and the schematic of the assembly is shown in Fig. 3. The arc-jet plasma source is housed inside a 508 mm diameter, 940 mm long, stainless steel vacuum chamber. Inside this chamber, a model movement system is located which is used to mount material samples or diagnostics probes. This system is discussed further in our accompanying publication [15]. The arc-jet is electrically isolated from the vacuum tank and thus on floating potential. The high current electric feedthroughs carry up to 500 A through isolated vacuum feedthroughs from the power supply to the plasma source. The test gas in the initial operation of the source is Argon which is delivered from a gas bottle by using a mass flow controller at a nominal mass flow rate of 0.2 g/s. Water cooling lines are in place inside the vacuum vessel to keep material temperatures under critical values. This includes one cooling circuit dedicated to the cathode, one dedicated to the anode, and one dedicated to the model movement system. In addition, a fourth cooling water circuit is used for a vacuum heat exchanger which will be described in more detail in section III.C.

Several facility measurements are taken to monitor the operational status of the plasma source. A mass flow metre is used to measure the cooling flow rate through the anode, and two thermocouples are used to determine the inlet and outlet temperature of this circuit which will allow the determination of the heat loss due to cooling of the anode. A mass flow controller is used to regulate the Argon mass flow rate, and two pressure sensors are used. One of these monitors the pressure in the stagnation chamber upstream of the arc-jet Laval nozzle, and the second monitors the vessel pressure, i.e. the approximate static pressure of the expanded plasma plume. In addition, PT100 and thermocouples will be placed on the arc-jet to monitor nozzle temperatures. Material samples may be equipped with thermocouples embedded to

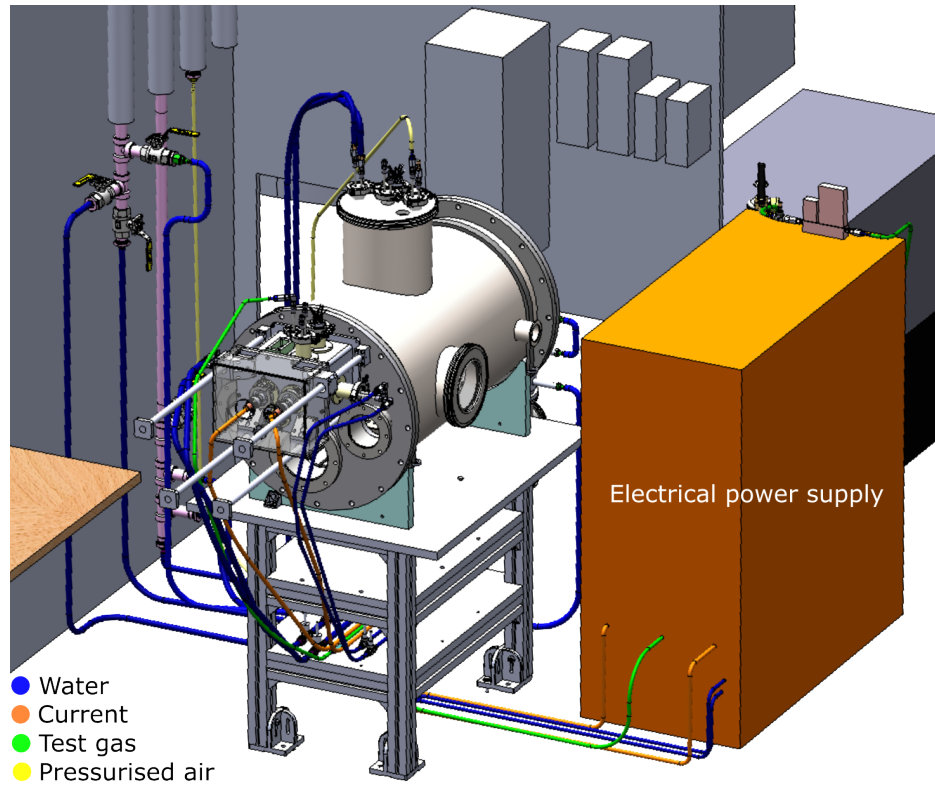


Fig. 1 Isometric view of the lab setup around OPG1.

measure their thermal performance when exposed to the plasma flow. All of the aforementioned measurements are collected in a National Instruments CDAQ data acquisition system. The power to the DAQ will be provided through an isolating transformer in order to reduce the noise from mains power when the plasma source is turned on.

The power is provided by a Jasic TIG 500P AC/DC tungsten inert gas (TIG) welding power supply capable of generating currents of up to 500 A and power of up to 21.5 kW. It will be used in DC TIG welding mode and a commercial welding torch is used as part of the bespoke plasma source. Operation of the power supply will be carried out by first setting the current manually on the power supply and then remotely turning on the facility. This is achieved with a bespoke control box connected to the power supply.

Several safety precautions are in place to protect personnel. All water and gas connections to the plasma source are made from non-conductive plastic to inhibit electrical current flowing through these connections. The water lines and the vacuum vessel itself will be grounded to prevent build up of static electrical charge. All connections will be covered with an insulative sleeve to prevent any accidental contact of any conducting components. An acrylic plastic hood is present at the rear of the vessel to prevent personnel getting into contact with the connections. Windows into the vacuum vessel will be covered with dark cloth to prevent personnel being exposed to bright arc radiation. Surfaces directly exposed to the plasma will be clad in insulating material.

B. Plasma source

The plasma source is based on a similar arrangement as reported in Ref [16]. It consists of a commercial water cooled tungsten inert gas welding torch coupled to bespoke components forming the nozzle which is set to positive potential (anode). An overview of the arc-jet is shown in Fig. 4 and a cross-sectional view is presented in Fig. 5. The system is based on a commercial TIG welding torch which is used as the negative electrode. An arc between the two electrodes heats the Argon test gas which passes through the torch and subsequently through the converging-diverging nozzle. The nozzle consists of a converging section which houses the cathode and a diverging section with a throat to exit area ratio of 6.25 and an exit diameter of 15 mm.

The torch is mounted on a set of two linear shafts and can be moved freely in axial direction inside the vacuum

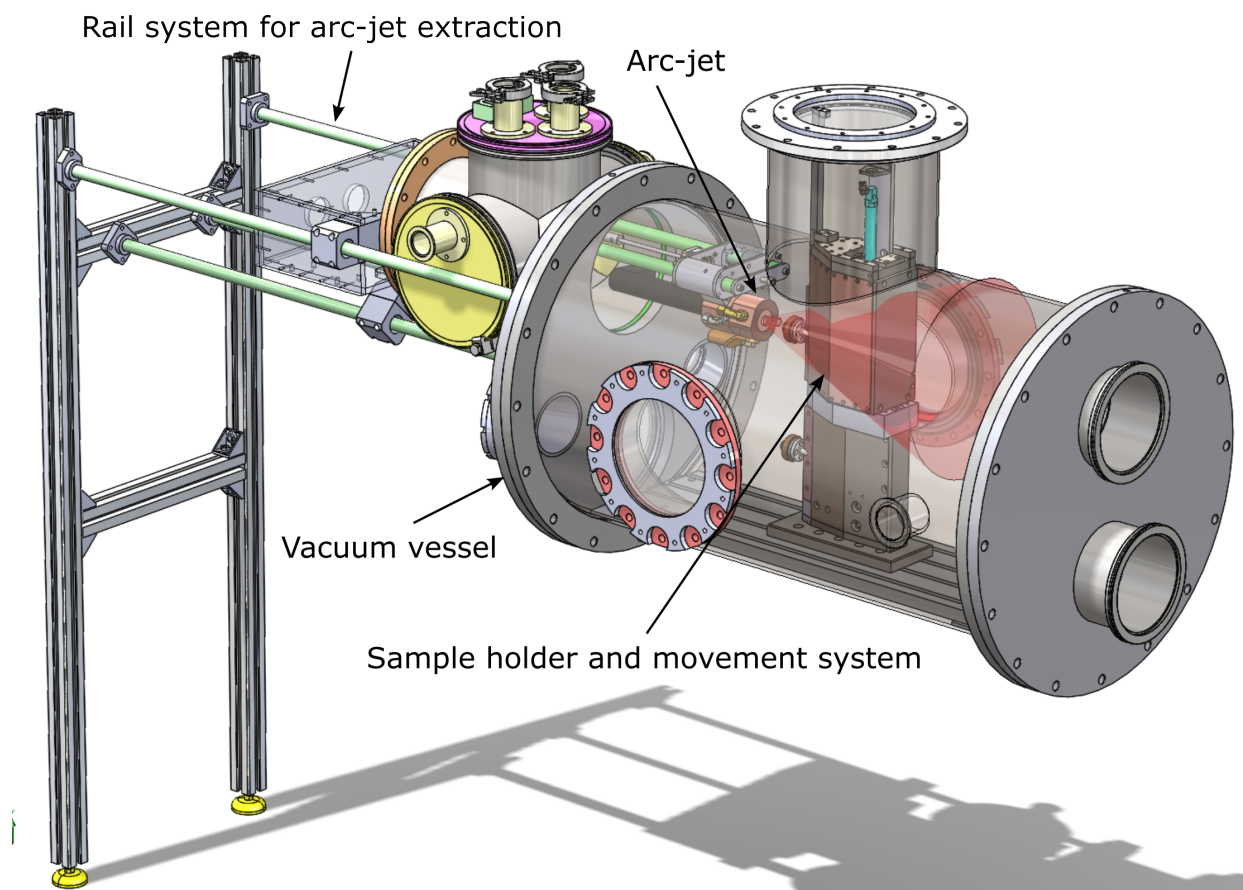


Fig. 2 Isometric view of the OPG1 plasma generator system.

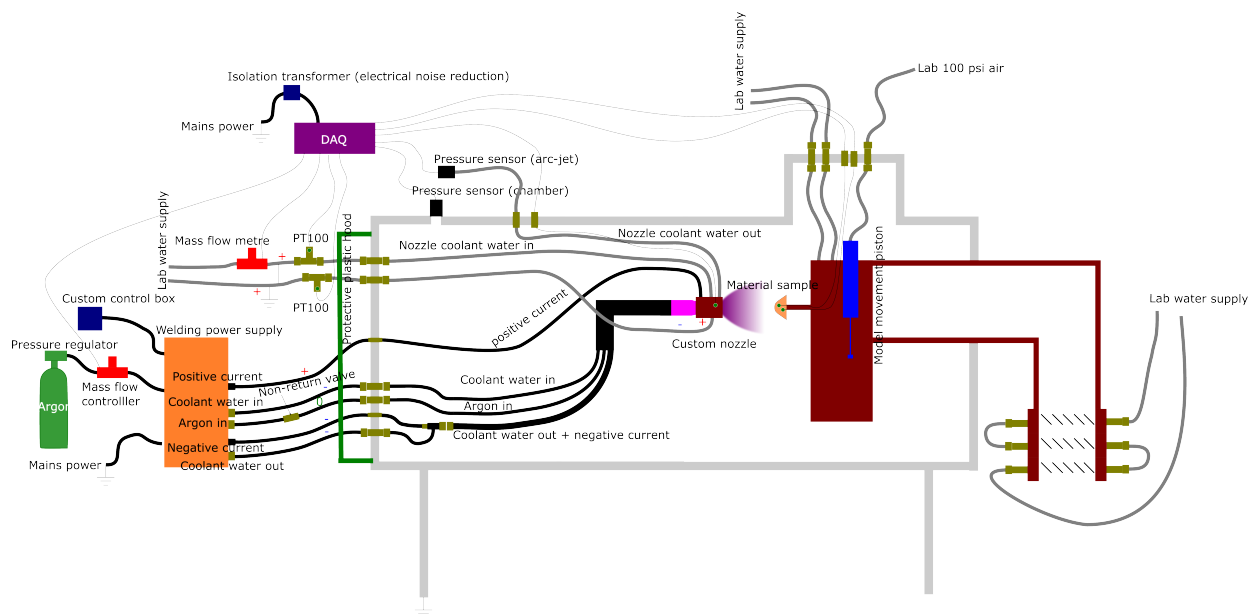


Fig. 3 Schematic overview of the OPG1 plasma generator system.

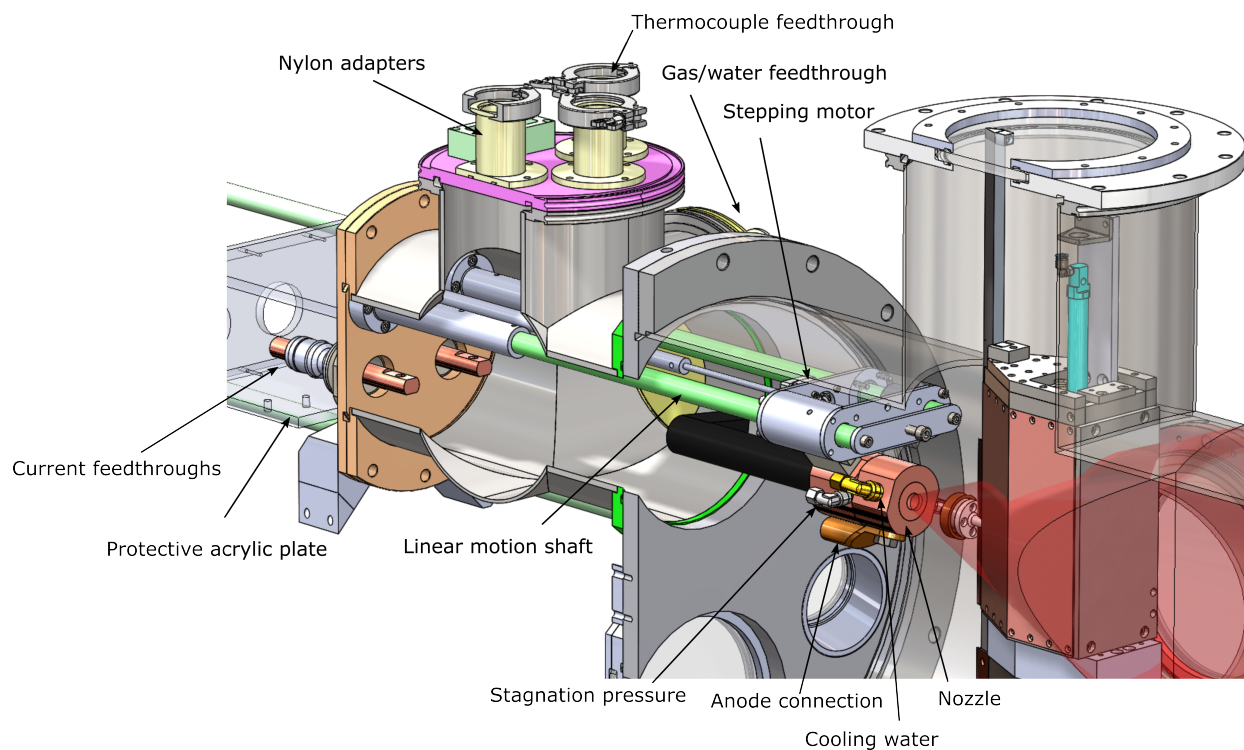


Fig. 4 Isometric view of arc-jet.

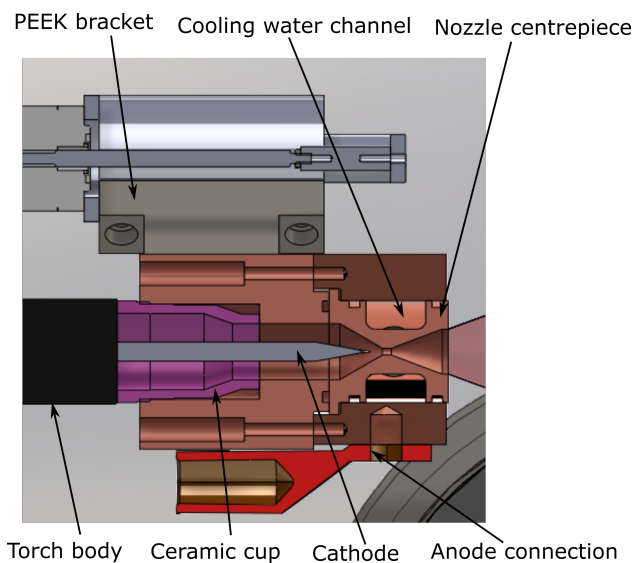


Fig. 5 Cross sectional view of arc-jet.

chamber using a stepping motor. The nozzle is water-cooled to prevent the melting of copper due to the heat produced by the electric arc. The maximum permissible time of this system is 200 s which is limited by the duty cycle parameters of the welding torch operated at maximum current. Starting of the torch functions by using a high-frequency current oscillation technique implemented in the welding power supply. Once the arc is formed it is maintained using DC power until the end of the test.

The plasma source is electrically isolated from the vessel for operational safety by preventing any possible point of contact between operator and equipment, as well as preventing the injection of electromagnetic noise into the

measurement infrastructure. All vacuum feedthroughs of power cables, measurement instrumentation, water lines, or gas feed systems are carried out by using a bespoke Nylon insulation piece between the feedthrough and the vacuum vessel. The body of the plasma torch is mounted on two PEEK brackets which insulate it thermally and electrically from the rest of the vessel. The way the system is set up, there is no electrically conductive connection between any two feedthroughs and no connection of any feedthrough to the vacuum vessel. This prevents instrumentation ground loops and the aforementioned electric noise. The back plate of the system is mounted on linear rails allowing easy access without removing the heavy front lid. The plasma source can slide backwards until the entire arc-jet is located outside the vacuum vessel. This enables a quick turnaround of inspection, maintenance or a change-over of parts without the need to move heavy components.

C. Vacuum System

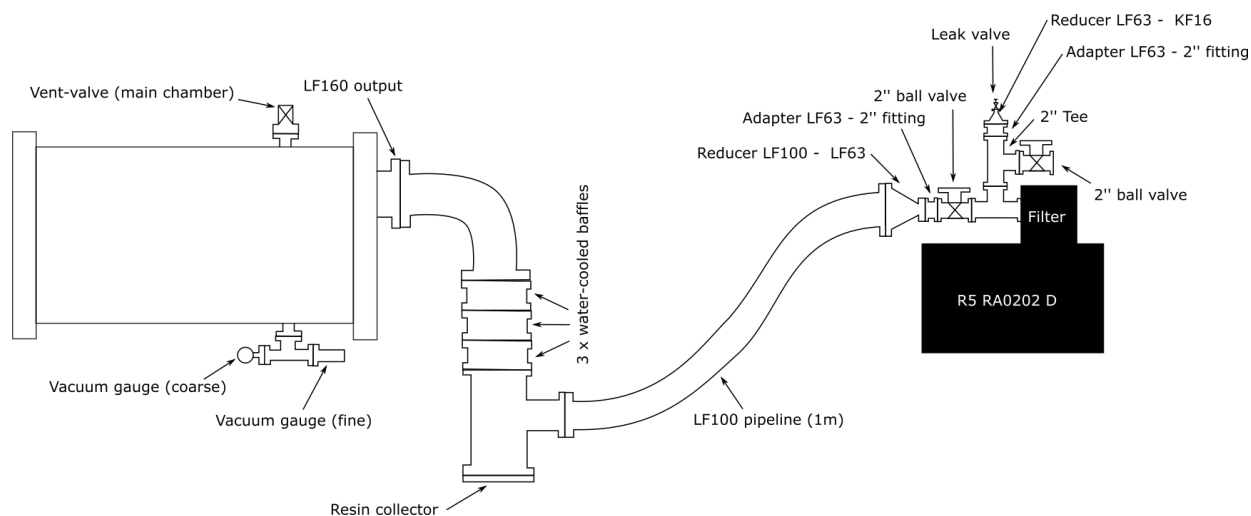


Fig. 6 Vacuum system schematic.



Fig. 7 Singular cold trap element.

The vacuum system is shown in Fig. 6 and consists of a series of 160 ISO-K components followed by a 100 ISO-K pipeline into a valve system housed at the Busch R5 RA0202 D pump. A ball valve can be used to isolate the pump and the vacuum chamber and an additional leak valve is present near the pump. It can also be used to artificially restrict the orifice area of the vacuum flow path, thus allowing a coarse control of the vacuum pressure inside the vessel. The leak valve adds a fine control by increasing the throughput of the pump and thus increasing the pressure inside the vacuum chamber. The flowpath is designed as short as possible and the pipe diameter is selected as large as possible to produce a high vacuum conductance. Three stainless steel heat exchanger units are present immediately downstream of the main chamber. Water-cooled diffusion pump baffles are used in series to cool the plasma flow before it enters the valve and pumping system. The challenge of these heat exchangers is to cool the flow significantly while not reducing the vacuum

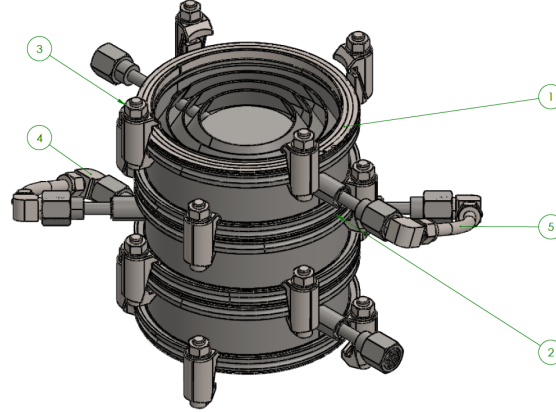


Fig. 8 Stack of three cold traps. (1) conical baffle, (2) ISO-K 160 connection, (3) clamp, (4) Elbow connector, (5) tubing.

conductance. They consist of angled baffles which turn the flow into one particular direction once it passes over them. These units are typically used at the inlet of diffusion pumps to prevent backflow of oil vapour by condensing it on their cooled conical baffles. Due to their design for a diffusion pump environment these units provide high vacuum conductivity which is crucial for this application. Three units in series are used to provide enough effective surface area for any remaining phenolic vapour to condense. The pumps may be damaged if these products are present in vapour form. A single unit is shown in Fig. 7, and the CAD model of the stacked assembly is shown in Fig. 8. The condensed resin may be extracted through a blind flange at the bottom of the vacuum system during facility maintenance.

D. Diagnostics

Figure 9 shows a schematic overview of the diagnostic setup which will be employed in the testing of material samples. A high-speed or conventional camera will view the model from the side to identify any high-frequency changes in the plasma flow, and serve as a basic monitoring means to observe the test. An Optris P1 M infrared camera will be used to view material samples from the front enabling surface temperature measurements. In addition, a fibre-coupled spectrometer will be used to measure the surface radiation emitted from any material samples. The spectrum collected through a combination of focussing optics and the fibre-coupled spectrometer will serve as an independent means to assess the surface temperature through back body spectral fitting. Two pressure sensors will be used to characterize the system: A vacuum gauge measuring the vessel pressure, and a sensor measuring the pressure in the stagnation chamber upstream of the converging section of the nozzle. Material samples can be equipped with in-depth thermocouples.

IV. System Design

This section summarises the design specific to different aspects of the system including electrical performance of a simple equivalent circuit, vacuum performance while injecting hot plasma, heat transfer of the arc in the nozzle throat, material ablation, and a computational fluid dynamics (CFD) analysis of the nozzle geometry and test sample. In following each of the different aspects are addressed.

A. Electrical circuit

An equivalent electrical circuit has been used to calculate the leakage currents through cooling water connections. The assumed conductivity of water was taken as $0.2 \Omega\text{m}$ which is a conservative value corresponding to ocean water, while copper is modelled with $1.7\text{E-}8 \Omega\text{m}$. The water line cross sectional area is based on 16 mm diameter tubes and the copper wire is based on a 120 mm^2 cross section of the power cable. For both water and copper wires, a total length of 1.5 m is assumed. The resistance is calculated via

$$R = \rho \frac{L}{A}, \quad (1)$$

with L corresponding to the wire length and A denoting the wire cross-sectional area. Resistances of vacuum

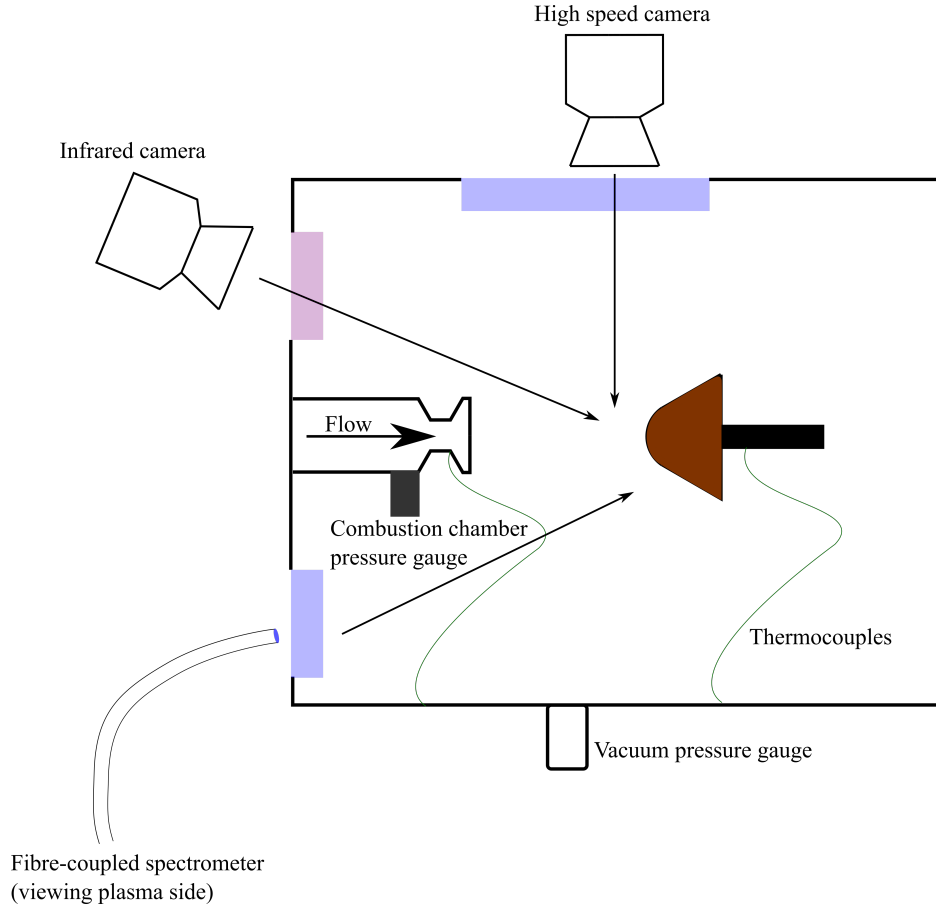


Fig. 9 Overview of the diagnostics used in OPG1.

feedthroughs have been omitted due to their large diameter and very short length. The resistance of the arc in the nozzle is assumed to be $R=0.008\Omega$, as this value generates the maximum power that can be drawn from the power supply while retaining the maximum possible current of 500 A. The circuit was solved for steady state DC operation in COMSOL Multiphysics using Kirchoff's circuit laws. The analysis showed that the leakage current to Earth is on the order of 3 mA and thus several orders of magnitude below the main power line, making the system efficient and safe to use.

B. Vacuum performance and cooling of plasma exhaust flow

A one-dimensional vacuum model has been constructed to analyse both the pump performance in terms of ultimate pressure as well as the heat transfer of the hot plasma flow to the vacuum system prior to the gas entry into the pump. An overview of the one-dimensional model is shown in Fig. 10. The vacuum system is partitioned into a series of equivalent volumes, and their conductances are lumped at the inlets. The analysis is carried out transiently, and the system reaches steady state within the first few seconds of operation. At steady state, the mass flow rate is \dot{m}_{in} throughout and the Argon temperature remains at the inlet value T_{in} until the entrance to the pipe. The pipe is divided into n equal volume elements with their conductances lumped at the inlets, such that for the i th pipe element, the pressure is $p_{pipe\ i}$, the rate of heat transfer to the surroundings is $\dot{Q}_{pipe\ i}$ and the Argon temperature at the exit is $T_{pipe\ i}$.

The pipe is assumed to be at ambient temperature $T_{amb} = 300$. Hence, the rate of heat transfer out of the i th pipe element can be found using the logarithmic mean temperature difference between the inlet and outlet Argon temperatures and the ambient temperature as per Equation 2 [17]. In this equation the quantity UA refers to the product of the overall heat transfer coefficient for the pipe and its outer surface area. The rate of heat transfer out of the element can also be expressed in terms of the temperature change of Argon using the steady flow energy equation as per Equation 3 where c_p is the constant pressure specific heat capacity of Argon.

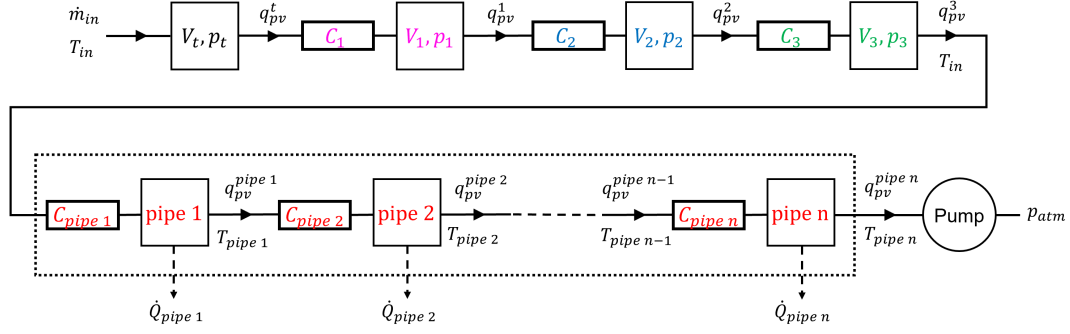


Fig. 10 Vacuum system model with heat loss.

$$\dot{Q}_{pipe\ i} = UA \left(\frac{(T_{pipe\ i-1} - T_{amb}) - (T_{pipe\ i} - T_{amb})}{\ln \left(\frac{T_{pipe\ i-1} - T_{amb}}{T_{pipe\ i} - T_{amb}} \right)} \right) \quad (2)$$

$$\dot{Q}_{pipe\ i} = -\dot{m}c_p (T_{pipe\ i} - T_{pipe\ i-1}) \quad (3)$$

The only thermal resistances considered are due to the pipe thickness and thermal boundary layer on the Argon side such that UA can be found using Equation 4 [17] where k_c is the thermal conductivity of copper, $L_{pipe\ i}$ is the length of the i th pipe element and r_1 and r_2 are the inner and outer radii of the pipe. The quantity h is the convective heat transfer coefficient on the Argon side and can be found from Nusselt number correlations in Equations 5 and 6 where the Reynolds number is given by $Re = \frac{2\dot{m}}{\pi r_1 \mu}$.

$$UA = \frac{2\pi l_{pipe\ i}}{\frac{1}{r_1 h} + \frac{\ln \left(\frac{r_2}{r_1} \right)}{k_c}} \quad (4)$$

$$Nu = 1.615 \left(\frac{Re\ Pr\ d}{l_{pipe\ i}} \right)^{\frac{1}{3}} ; \quad Re < 2000 \quad (5)$$

$$Nu = 0.023 Re^{0.8} Pr^{0.4} ; \quad Re > 2000 \quad (6)$$

Equations 2 and 3 can be combined to give Equation 8 which relates the Argon temperatures at the inlet and outlet of the i th pipe element. Starting at the pipe inlet where the Argon temperature is known, Equation 8 can be used to step between elements to find the steady state temperature distribution across the pipe. The temperature at the vacuum pump inlet is $T_{pipe\ n}$ such that the required pump throughput is $q_{pv}^{pipe\ n} = \dot{m}_{in} RT_{pipe\ n}$. The vacuum pump characteristic given by the manufacturer and

$$q_{pv} = pS \quad (7)$$

give a unique pump inlet pressure $p_{pump} = p_{pipe\ n}$ corresponding to this throughput. The pressure across the pipe can be found by starting at the known pump inlet pressure and stepping backwards between pipe elements using Equation 9. Calculating the conductance $C_{pipe\ i}$ requires knowledge of both pressures $p_{pipe\ i-1}$ and $p_{pipe\ i}$, but the former value is initially unknown. Therefore, an initial guess is made for $p_{pipe\ i-1}$ to calculate $C_{pipe\ i}$ and then this updates the value of $p_{pipe\ i-1}$ using Equation 9, converging to the solution. The pressure $p_{pipe\ -1}$ is equivalent to p_3 such that Equation 10 can be used to find the remaining pressures.

$$T_{pipe\ i} = T_{amb} + e^{-\frac{UA}{\dot{m}_{in} c_p}} (T_{pipe\ i-1} - T_{amb}) \quad (8)$$

$$p_{pipe\ i-1} = p_{pipe\ i} + \frac{\dot{m}_{in} RT_{pipe\ i-1}}{C_{pipe\ i}} \quad (9)$$

$$p_t = p_1 + \frac{\dot{m}_{in}RT_{in}}{C_1} ; \quad p_1 = p_2 + \frac{\dot{m}_{in}RT_{in}}{C_2} ; \quad p_2 = p_3 + \frac{\dot{m}_{in}RT_{in}}{C_3} \quad (10)$$

Running this model gave a steady state pressure of 58.31Pa in the test volume and a steady state pump inlet temperature of 352.39K while a constant injection of 0.2 g/s Argon plasma took place. This model does not include the cooling effect due to the heat exchanger baffles and therefore represents a conservative estimate of the pump inlet temperature. The solution was verified to be insensitive to the choice of n for sufficiently large values of n . The target pressure of 125Pa can be achieved by operating a ball valve and hence artificially changing the vacuum line orifice area.

C. Heat transfer in plasma generator

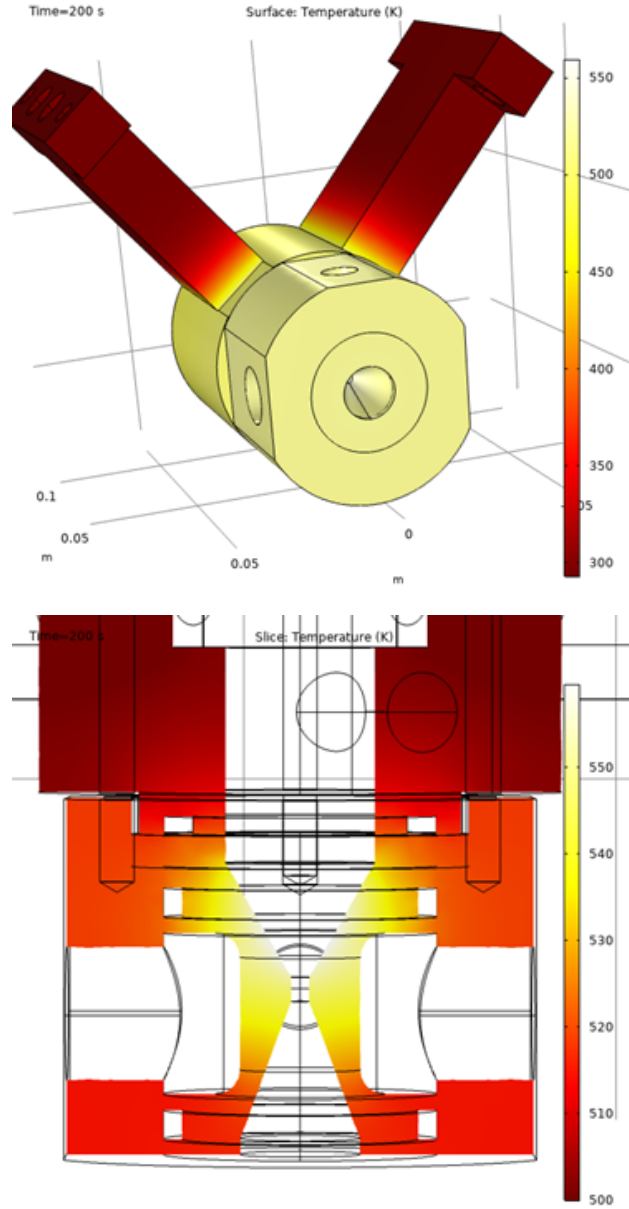


Fig. 11 Heat transfer simulation of nozzle assembly.

A transient 3D heat transfer analysis was conducted using the commercial Multiphysics tool COMSOL. In order to

model the heat transfer from the arc into the copper nozzle a constant heat input over the converging part of the nozzle was assumed providing the maximum power of the system, i.e. 20.15 kW, and adjusting it with an estimated efficiency of 0.5. As Peichl and Auweter-Kurtz et al. found an efficiency between 0.65 and 0.9 for a similar design [16, 18], 0.5 was selected in the current work as a conservative estimate. The cooling effectiveness of the water line is modelled around the central part of the nozzle by treating this area as a cylinder in a cross flow. With an assumed water mass flow rate of 0.01 kg/s, this amounts to a flow velocity of 0.033 m/s. Using a viscosity value of $\mu = 7.97\text{E-}4$ Pa s for water at ambient conditions, a Reynolds number of $\text{Re} = 627$ is obtained. Within this range the Nusselt correlation

$$\text{Nu} = 0.583 \text{Re}^{0.471} \quad (11)$$

is appropriate resulting in a heat transfer coefficient of $h = 499 \text{ W m}^{-2} \text{ K}^{-1}$ when a water thermal conductivity of $k = 0.618 \text{ W m}^{-1} \text{ K}^{-1}$ is used. This water cooling heat transfer was applied using a convective cooling term by assuming a constant water temperature of 320 K in the circumference of the water channel. The convective heat transfer of plasma flow to the nozzle wall was modelled using a Nusselt correlation for circular pipe flow in the laminar regime. $\text{Nu} = 4.36$ was assumed, resulting in a heat transfer coefficient of $7.75 \text{ W m}^{-2} \text{ K}^{-1}$. A plasma temperature of 5000 K was assumed to be the driving temperature in this case.

A transient simulation using a tetrahedral mesh of 216,000 cells was conducted up to 200 s duration. All materials used were assumed to be copper using the inbuilt material library which accounts for temperature-dependent thermophysical properties. The only exception are the PEEK mounting brackets which both thermally and electrically isolate the system from the remaining facility. The resulting temperature distributions at the last time step (200 s) are shown in Fig. 11. Temperatures remain below 560 K throughout, preventing any melting of the copper structure. O-rings will be made from FFKM material which can tolerate temperatures of up to 600 K and therefore suffice in this design.

D. Test sample material ablation

Materials planned for initial tests are P50 cork, Calcarb and Graphite. These represent a real heat shield material, a charred carbon fibre structure and a solid carbon body. It is envisioned to investigate differences in ablative behaviour by comparing these different material types. Material ablation will cause particulates and phenolic vapour to be injected into the vacuum system. Some of the resulting products of the phenolic resin may be hazardous and an analysis below is presented estimating the amount of produced phenolic vapour.

Using the results obtained in Ref [19] a conservative value of 5 % per minute rate of change in mass is assumed. The envisioned sample geometry amounts to approximately 0.3 g of ablated cork material during a test run. The ablated cork will partially condense in the heat exchanger units and the remaining gas will travel through the pumping system and into the laboratory vacuum exhaust line. The heavily diluted gas passes through a filter outside the building and is released into the atmosphere. The composition of this gas can be estimated using the simulation results from Ref [20] showing that the major species at cooled ambient conditions are CH_4 , CO_2 and CO . Using the approximate results discussed above, the diluted mole fractions at the filter vent to atmosphere are $1.3\text{E-}3$, $7.7\text{E-}4$, and $2.6\text{E-}5$ respectively, all of which are far below dangerous levels.

E. Nozzle flow

Initial simulations of the nozzle flow with a 40 mm diameter test-model (45 degree sphere-cone) have been carried out using Eilmer 4 [21]. Argon is modelled as a viscous reacting gas and the simulation includes ionized Argon and free electrons. In total, ten simulations have been carried out with varying total temperature and chamber pressure. The total temperatures computed are 3700 K and 7400 K, while the chamber pressures are 17 Pa, 50 Pa, 125 Pa, 300 Pa, and 600 Pa. Figure 12 shows the temperature and velocity distributions of the simulated domain. The inlet mass flux boundary condition provides 0.2 g/s on the left hand side of Fig. 12. These values are based on the work presented in Ref [16]. The right hand side represents the vacuum chamber and is modelled using a simple outflow boundary condition with a constant pressure. These different pressure values span possible test flow conditions that would be required to achieve the acceleration tube fill pressure of the expansion tube condition as explained in [22]. All other walls are modelled as no slip walls in this initial study. In the case of $T_0 = 3700 \text{ K}$ and $p = 125 \text{ Pa}$ a Mach number of approximately 3 is reached at the exit and the plasma flow is over-expanded which leads to the slight oblique shock visible in the velocity magnitude trace of Fig. 12. The supersonic flow impinges on the test model front and expands around the conical section after a detached shock is formed in front of the capsule model. As the chamber pressure is increased, the overexpansion is stronger and hence the oblique recompression shock is also stronger. At the lowest computed pressure of 17 Pa, the flow is underexpanded and the free jet envelops a larger portion of the model. Sample heat flux distributions along the

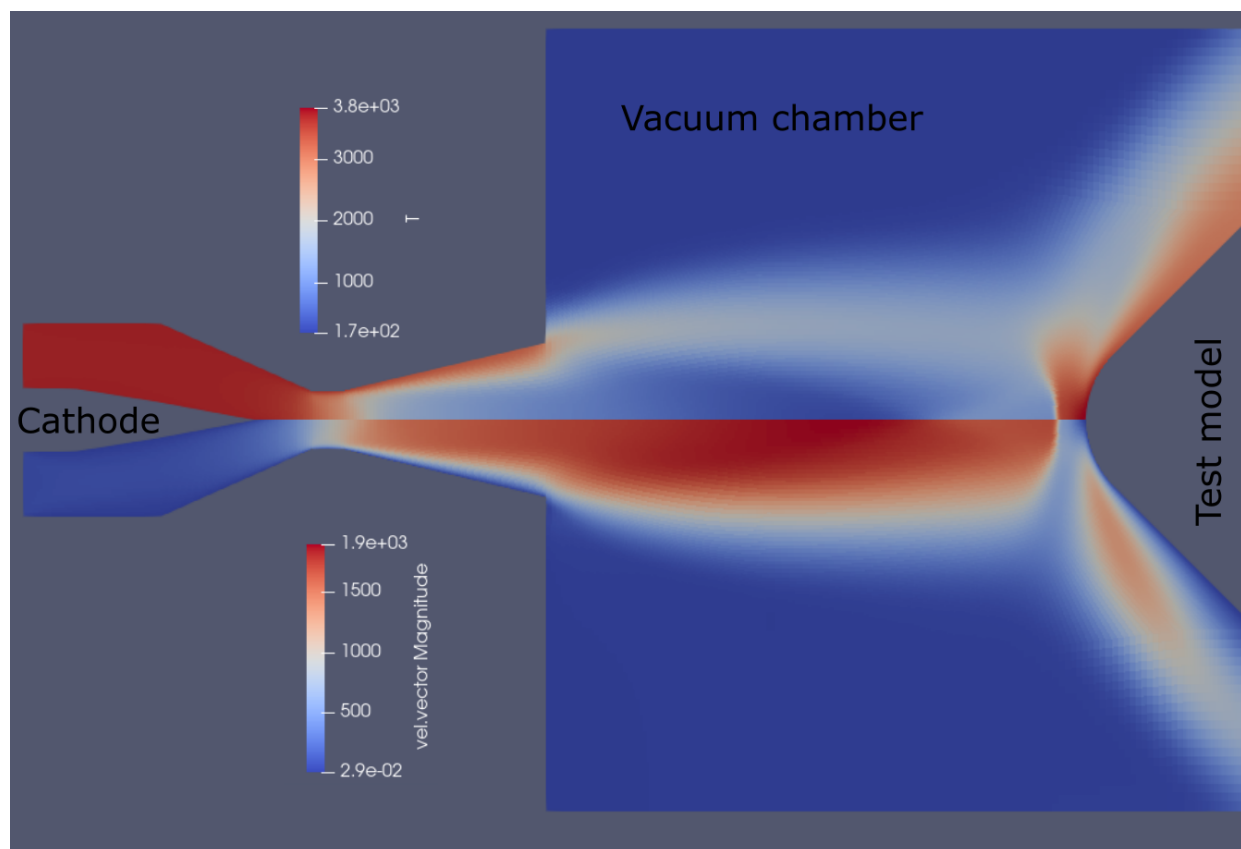


Fig. 12 CFD simulation of nozzle for $T_0 = 3700$ K and $p = 125$ Pa (top: temperature in K, bottom: velocity magnitude in m/s).

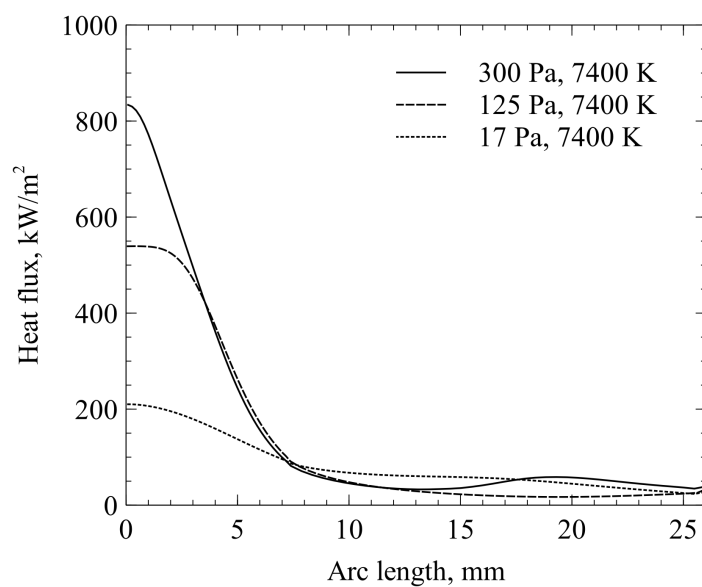


Fig. 13 Heat flux distribution along test model surface. Arc length starts at model nose, i.e. stagnation point.

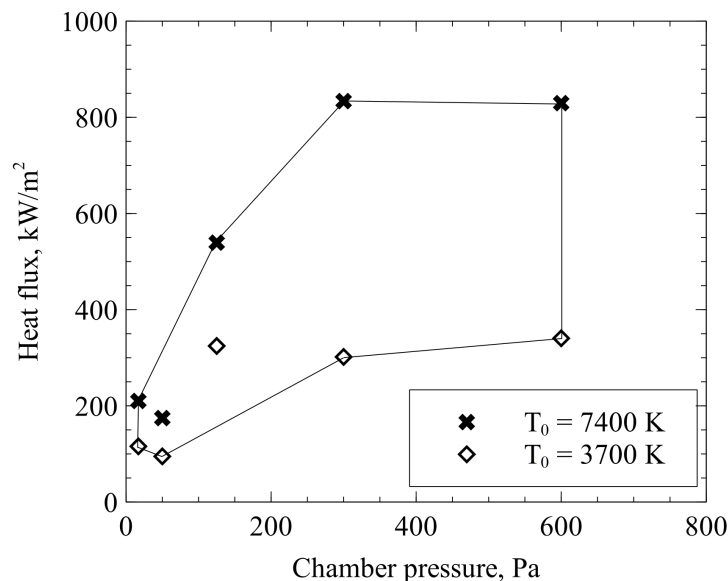


Fig. 14 Estimated envelope of heat flux as a function of chamber pressure and total temperature.

test model are shown in Fig. 13. The estimated facility performance envelope of simulated maximum heat flux is shown in Fig. 14. For a test sample under radiation adiabatic conditions with an emissivity of 0.85 this envelope relates to achievable surface temperatures between 1180 K and 2040 K.

V. Conclusion

This paper discusses the development of a stand-alone, small-scale 21.5kW arc-jet facility. An arc-jet is situated inside a vacuum vessel forming a high enthalpy Argon plasma. It is electrically isolated from the vessel and any instrumentation to reduce noise in the measured quantities of massflow, temperature and pressure. The vessel is evacuated by a series of pumps providing sufficient suction to keep the vessel below 125 Pa during continuous injection of 0.2 g/s of plasma. Planned plasma diagnostics include spectroscopic optical measurements and filtered imaging using conventional cameras. The system is designed with regards to heat transfer, vacuum performance, and material ablation keeping relevant parameters below critical values. A viscous reacting 2D axisymmetric simulation of the nozzle flow up to the model surface showed that a Mach number of approximately 3 could be reached at the plasma entry into the vacuum chamber. The next step in the development cycle of this facility is a series of commissioning tests which will allow the first characterisation of the plasma facility.

Acknowledgments

This research was funded in whole by the UKRI Future Leaders Fellowship scheme (grant number MR/T041269/1) and we extend our gratitude to UKRI. For the purpose of Open Access, the author has applied a CC BY public copyright licence to any Author Accepted Manuscript (AAM) version arising from this submission. We also thanks Megan MacDonald and Joe Hartman for their help in discussing our design and sharing their experience of the mARC II facility with us. We extend our gratitude to Christopher Johnston for providing us with trajectory conditions for the planned Mars sample return mission. We would also like to thank Marko Bacic and Paul Beard for lending us a vacuum pump and Peter Collen for providing the idea of a resin collector in the vacuum system.

References

- [1] Loehle, S., Fabian, Z., Eberhart, M., Hermann, T., Meindl, A., Massuti-Ballester, B., Leiser, D., Hufgard, F., Pagan, A., Herdrich, G., and Fasoulas, S., "Assessment of high enthalpy flow conditions for re-entry aerothermodynamics in the plasma

wind tunnel facilities at IRS,” *CEAS Space Journal*, 2021.

- [2] Inman, J., Bathel, B., Johansen, C., Danehy, P., Jones, S., Gragg, J., and Splinter, S., “Nitric Oxide PLIF Measurements in the Hypersonic Materials Environmental Test System (HYMETS),” *49th AIAA Aerospace Sciences Meeting Including the New Horizons Forum and Aerospace Exposition*, 2011. <https://doi.org/10.2514/6.2011-1090>.
- [3] Balter-Peterson, A., Nichols, F., Misfud, B., and Wendell, L., “Arc jet testing in NASA Ames Research Center thermophysics facilities,” No. 0 in Meeting Paper Archive, American Institute of Aeronautics and Astronautics, 1992. <https://doi.org/10.2514/6.1992-5041>, URL <https://doi.org/10.2514/6.1992-5041>.
- [4] Bottin, B., Chazot, O., Carbonaro, M., Haegen, V., and Paris, S., “The VKI Plasmatron Characteristics and Performance,” 2000, p. 26.
- [5] De Filippis, F., “SCIROCCO PWT Facility for High Temperature Resistant Material Assemblies Tests,” No. 0 in International Astronautical Congress (IAC), American Institute of Aeronautics and Astronautics, 2003. <https://doi.org/10.2514/6.IAC-03-I.3.04>, URL <https://doi.org/10.2514/6.IAC-03-I.3.04>.
- [6] Bonvoisin, B., Meisnar, M., Merrifield, J., Beck, J., Lips, T., Guelhan, A., Schleutker, T., Herdrich, G., Pagan, A., Kaschnitz, E., Liedtke, V., Helber, B., Lopes, S., Gouriet, J. B., Chazot, O., and Ghidini, T., “Demisability assessment of space materials,” *CEAS Space Journal*, 2022. <https://doi.org/10.1007/s12567-022-00429-0>, URL <https://doi.org/10.1007/s12567-022-00429-0>.
- [7] MacDonald, M. E., Jacobs, C. M., Laux, C. O., Zander, F., and Morgan, R. G., “Measurements of Air Plasma/Ablator Interactions in an Inductively Coupled Plasma Torch,” *Journal of Thermophysics and Heat Transfer*, Vol. 29, No. 1, 2014, pp. 12–23. <https://doi.org/10.2514/1.T4402>, URL <https://doi.org/10.2514/1.T4402>.
- [8] Kolesnikov, A. F., “The Concept of Local Simulation for Stagnation Point Heat Transfer in Hypersonic Flows: Applications and Validation,” *21st AIAA Aerodynamic Measurement and Ground Testing Conference*, Denver, CO, 2000.
- [9] MacDonald, M. E., Philippidis, D., Ho, T., Haw, M., Hartman, J., and McGlaughlin, M., “Build-up of the second-generation 30 kW miniature arc jet (mARC II) at NASA Ames Research Center,” No. 0 in AIAA AVIATION Forum, American Institute of Aeronautics and Astronautics, 2019. <https://doi.org/10.2514/6.2019-2857>, URL <https://doi.org/10.2514/6.2019-2857>.
- [10] Wang, L., Xing Han, X., Sheng Long, Y., and Chen, W., “Electrode Erosion of Arc Heater by Emission Spectroscopy,” *Journal of Thermophysics and Heat Transfer*, Vol. 36, No. 2, 2021, pp. 291–295. <https://doi.org/10.2514/1.T6326>, URL <https://doi.org/10.2514/1.T6326>.
- [11] Luís, D., and MacDonald, M. E., “Emission spectroscopy characterization of electrode species in the freestream flow at the NASA Ames miniature Arc Jet II facility,” *Journal of Quantitative Spectroscopy and Radiative Transfer*, Vol. 272, 2021, p. 107752. <https://doi.org/10.1016/j.jqsrt.2021.107752>, URL <https://www.sciencedirect.com/science/article/pii/S0022407321002454>.
- [12] Nawaz, A., Ho, T. S., Philippidis, D., MacDonald, M., McGlaughlin, M. S., and Driver, D. M., “Baseline characterization of the 30kW miniature arc jet facility mARC at NASA Ames,” No. 0 in AIAA AVIATION Forum, American Institute of Aeronautics and Astronautics, 2016. <https://doi.org/10.2514/6.2016-3819>, URL <https://doi.org/10.2514/6.2016-3819>.
- [13] Odion Iyinomen, D., Malpress, R., and Buttsworth, D., “Technique Development for Investigating Axisymmetric Ablation Models in Hypersonic Impulse Facilities,” *AIAA Journal*, Vol. 59, No. 6, 2020, pp. 1899–1913. <https://doi.org/10.2514/1.J059629>, URL <https://doi.org/10.2514/1.J059629>.
- [14] Mundt, C., “Development of the New Piston-Driven Shock-Tunnel HELM,” *Experimental Methods of Shock Wave Research*, edited by O. Igra and F. Seiler, Springer International Publishing, Cham, 2016, pp. 265–283. https://doi.org/10.1007/978-3-319-23745-9_8, URL https://doi.org/10.1007/978-3-319-23745-9_8.
- [15] Chang, E. W. K., Joglekar, C., McGilvray, M., and Hermann, T., “Integration of Arcjet in Impulse Facility for Hypervelocity Aerothermal Testing with Ablation,” *AIAA SciTech*, 2023.
- [16] Peichl, J., “Characterization of a miniature arcjet heater,” Master’s thesis, Institute of Space Systems, University of Stuttgart, 2019.
- [17] Rogers, G., and Mayhew, Y., *Engineering Thermodynamics Work and Heat Transfer, 3rd Edition*, Longman, 1980.
- [18] Auweter-Kurtz, M., Kurtz, H. L., and Laure, S., “Plasma generators for re-entry simulation,” *Journal of Propulsion and Power*, Vol. 12, 1996, pp. 1053–1061.

- [19] Sakraker, I., Chazot, O., and Carvalho, J. P., “Performance of cork-based thermal protection material P50 exposed to air plasma,” *CEAS Space Journal*, Vol. 14, No. 2, 2022, pp. 377–393. <https://doi.org/10.1007/s12567-021-00395-z>, URL <https://doi.org/10.1007/s12567-021-00395-z>.
- [20] Rabinovitch, J., Marx, V., and Blanquart, G., *Pyrolysis Gas Composition for a Phenolic Impregnated Carbon Ablator Heatshield*, 2014. <https://doi.org/10.2514/6.2014-2246>.
- [21] Jacobs, P., and Gollan, R., “Implementation of a Compressible-Flow Simulation Code in the D Programming Language,” *Applied Mechanics and Materials*, Vol. 846, 2016, pp. 54–60. <https://doi.org/10.4028/www.scientific.net/AMM.846.54>.
- [22] Chang, E. W. K., Hermann, T., McGilvray, M., and James, C. M., “Mars Sample Return Condition Design and Testing in T6 Stalker Tunnel,” *9th International Workshop on Radiation of High Temperature Gases for Space Missions*, 2022.